Neuron

Article

Divergent Neural Pathways Emanating from the Lateral Parabrachial Nucleus Mediate Distinct Components of the Pain Response

Highlights

- The lPBN mediates escape and aversion to noxious stimuli
- Spatially segregated neurons in the lPBN collateralize to distinct targets
- Distinct output pathways give rise to separate aspects of the pain response

Authors

Michael C. Chiang, Eileen K. Nguyen, Martha Canto-Bustos, Andrew E. Papale, Anne-Marie M. Oswald, Sarah E. Ross

Correspondence

saross@pitt.edu

In Brief

Chiang et al. reveal that neurons in spatially segregated regions of the lateral parabrachial nucleus collateralize to distinct targets and that activation of distinct efferents gives rise to separate components of the nocifensive response.

Chiang et al., 2020, Neuron *106*, 927–939
June 17, 2020
https://doi.org/10.1016/j.neuron.2020.03.014

CellPress

Neuron

CellPress

Article

Divergent Neural Pathways Emanating from the Lateral Parabrachial Nucleus Mediate Distinct Components of the Pain Response

Michael C. Chiang,[1,2] Eileen K. Nguyen,[1,2] Martha Canto-Bustos,[3] Andrew E. Papale,[1] Anne-Marie M. Oswald,[3,4] and Sarah E. Ross[1,2,4,5,*]

[1]Department of Neurobiology, University of Pittsburgh, Pittsburgh, PA 15213, USA
[2]Pittsburgh Center for Pain Research, University of Pittsburgh, Pittsburgh, PA 15213, USA
[3]Department of Neuroscience, University of Pittsburgh, Pittsburgh, PA 15213, USA
[4]Center for the Neural Basis of Cognition, Pittsburgh, PA, USA
[5]Lead Contact
*Correspondence: saross@pitt.edu
https://doi.org/10.1016/j.neuron.2020.03.014

SUMMARY

The lateral parabrachial nucleus (lPBN) is a major target of spinal projection neurons conveying nociceptive input into supraspinal structures. However, the functional role of distinct lPBN efferents in diverse nocifensive responses have remained largely uncharacterized. Here we show that that the lPBN is required for escape behaviors and aversive learning to noxious stimulation. In addition, we find that two populations of efferent neurons from different regions of the lPBN collateralize to distinct targets. Activation of efferent projections to the ventromedial hypothalamus (VMH) or lateral periaqueductal gray (lPAG) drives escape behaviors, whereas activation of lPBN efferents to the bed nucleus *stria terminalis* (BNST) or central amygdala (CEA) generates an aversive memory. Finally, we provide evidence that dynorphin-expressing neurons, which span cytoarchitecturally distinct domains of the lPBN, are required for aversive learning.

INTRODUCTION

The central nervous system has evolved to promote behavioral adaptations and physiological responses to maintain homeostasis under varying environmental conditions. In particular, the lateral parabrachial nucleus (lPBN) has been established to play a key role in maintaining homeostasis under stressful or threatening circumstances (Palmiter, 2018; Saper, 2016). The lPBN responds robustly to food neophobia, hypercapnia, and threat by eliciting protective behaviors (Campos et al., 2018; Chamberlin and Saper, 1994; Kaur et al., 2013, 2017). In addition, the lPBN also has a significant role in nociceptive behavior and long-term behavioral changes in response to painful stimuli (Campos et al., 2018; Han et al., 2015). Thus, the lPBN must integrate a myriad of exteroceptive and interoceptive signals with autonomic regulation to permit an appropriate behavioral response under stressful circumstances, such as threat or injury, to ensure an animal's survival (Chiang et al., 2019).

A critical response to threats includes innate behaviors that allow an animal to escape from and remember noxious or threatening experiences (Espejo and Mir, 1993; Fan et al., 1995; Kunwar et al., 2015; Le Bars et al., 2001; Wang et al., 2015). Previous studies have established that the lPBN is a primary target for nociceptive information arising from the spinal cord (Al-Khater and Todd, 2009; Todd et al., 2000). Indeed, the majority of lPBN neurons respond to noxious stimuli (Bester et al., 1997; Hermanson and Blomqvist, 1996, 1997; Jansen and Giesler, 2015; Menendez et al., 1996). Recently, the contribution of a specific subpopulation of lPBN neurons expressing the calcitonin gene-related peptide (CGRP) has been demonstrated to have important roles in fear learning and encoding of danger signals (Campos et al., 2018). Additional populations expressing the neuropeptide substance P have been implicated in affective as well as reflexive behaviors to noxious stimuli (Barik et al., 2018; Huang et al., 2019). However, these subpopulations represent only a small portion of lPBN neurons. Given that lPBN neurons respond to noxious stimulation and contribute to appropriate behavioral responses for survival, we sought to gain a clearer understanding of lPBN efferents and how their activity might contribute to the response to noxious stimuli.

In this study, we investigated the varying contributions of distinct lPBN efferents to the bed nucleus *stria terminalis* (BNST), central amygdala (CEA), ventromedial hypothalamus (VMH), and lateral periaqueductal gray (lPAG). Chemogenetic inhibition revealed the requirement of the lPBN in nocifensive behavior. Furthermore, we found that subsets of neurons in spatially segregated regions within the lPBN collateralize to distinct targets. Optogenetic manipulation of these specific outputs recapitulates specific components of a nocifensive response. Furthermore, we characterize a previously unspecified local lPBN circuit involving dynorphin neurons that are activated by noxious stimuli and may convey this information across lPBN subdivisions to mediate aversion.

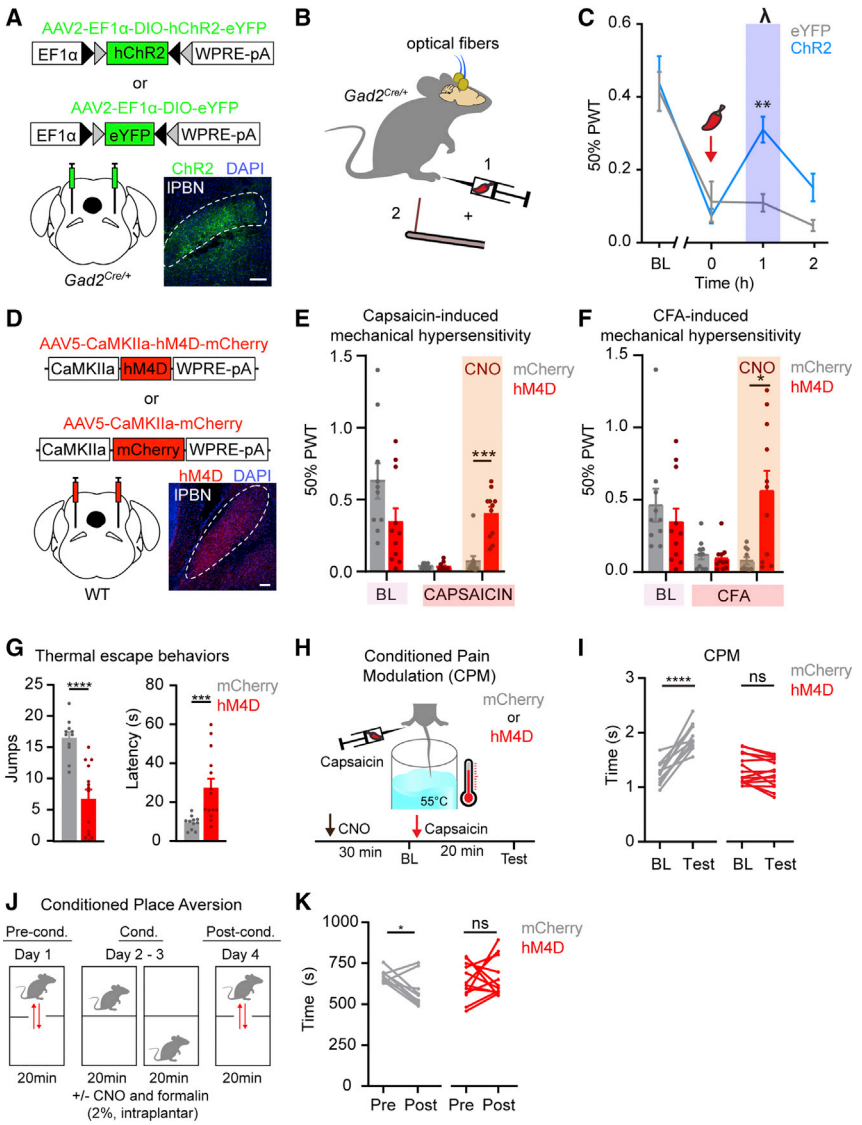

Figure 1. IPBN Is Required for Numerous Behavioral Responses to Noxious Stimuli

(A) Strategy to inhibit the IPBN through activation of inhibitory neurons. Shown is a representative image of ChR2 within the IPBN (outline). Scale bar, 100 μm.

(B) Mechanical hypersensitivity was (1) induced through intraplantar injection of capsaicin (10 μL, 0.03%) and (2) tested using von Frey filaments.

(C) The paw withdrawal threshold (PWT) was significantly reduced during optogenetic stimulation (blue bar) in ChR2 mice compared with eYFP mice in a model of capsaicin-induced mechanical hypersensitivity. Data are mean ± SEM (n = 10–11 mice per group). Two-way repeated measures (RM) ANOVA followed by Holm-Sidak post hoc test, $^{**}p < 0.01$.

(D) Strategy to inhibit the IPBN through inhibition of excitatory neurons.

(E) The PWT was significantly increased following intraperitoneal (i.p.) injection of CNO (orange bar) in hM4D mice compared with mCherry controls in a model of capsaicin-induced mechanical hypersensitivity. Data are mean ± SEM (n = 10–11 mice per group). Two-way RM ANOVA followed by Holm-Sidak post hoc test, $^{***}p < 0.001$.

(F) The PWT was significantly increased following i.p. injection of CNO (orange bar) in hM4D mice compared with mCherry controls in a model of CFA-induced mechanical hypersensitivity. Testing was performed 7 days post-CFA treatment. Data are mean ± SEM (n = 10–11 mice per group). Two-way RM ANOVA followed by Holm-Sidak post hoc test, $^{*}p < 0.05$.

(G) Escape behaviors from a 55°C plate increased significantly following i.p. injection of CNO in hM4D mice (red bars) compared with mCherry controls (gray bars). Data are mean ± SEM (n = 11–14 mice per group); $^{***}p < 0.001$, $^{****}p < 0.001$ (Student's t test).

(H) Strategy to test for conditioned pain modulation (CPM) using intraplantar capsaicin (0.03%).

(I) CPM was observed in mCherry control mice but not hM4D mice (n = 11–14 mice per group). $^{****}p < 0.0001$; not significant (ns), $p > 0.05$ (paired Student's t test).

(J) Protocol for conditioned place aversion (CPA). CNO was given 30 min prior to 2% intraplantar formalin on days 2 and 3, which was paired with one side of a two-chambered box differentiated by visual cues.

(K) Formalin-induced CPA is observed in control mice but not in those expressing hM4D (n = 11–14 mice per group). $^{****}p < 0.0001$); ns, $p > 0.05$ (paired Student's t test).

RESULTS

Nociceptive information is conveyed from the spinal cord to multiple regions of the brain in parallel, including brain stem, midbrain, and forebrain structures (Todd, 2010). Although the lPBN is a major target of the anterolateral tract in murine species (Cameron et al., 2015; Todd, 2010; Todd et al., 2000), its relative contribution to pain behaviors has only recently been explored (Alhadeff et al., 2018; Barik et al., 2018; Huang et al., 2019; Rodriguez et al., 2017). To further address this issue, we tested whether transiently inhibiting the lPBN would affect the behavioral response to noxious stimuli using adeno-associated virus (AAV)-mediated expression of channelrhodopsin2 (ChR2) in *Gad2*^{Cre} neurons to enable light-activated inhibition (Figures 1A and 1B). Dual fluorescence *in situ* hybridization (FISH) experiments confirmed that Gad2-expressing neurons co-expressed *Vgat* (*Slc32a1*) but not *Vglut2* (*Slc17a6*) throughout the lPBN (Figure S1). In the absence of light, ChR2 and enhanced yellow fluorescent protein (eYFP) mice showed capsaicin-induced mechanical hypersensitivity. However, this hypersensitivity was significantly reduced when inhibitory neurons in the lPBN were photostimulated (Figure 1C). As an alternative approach to inhibit the lPBN, we also expressed an inhibitory (hM4D) designer receptors exclusively activated by designer drugs (DREADD) in excitatory neurons in the lPBN (Figure 1D). Treatment of mice with clozapine N-oxide

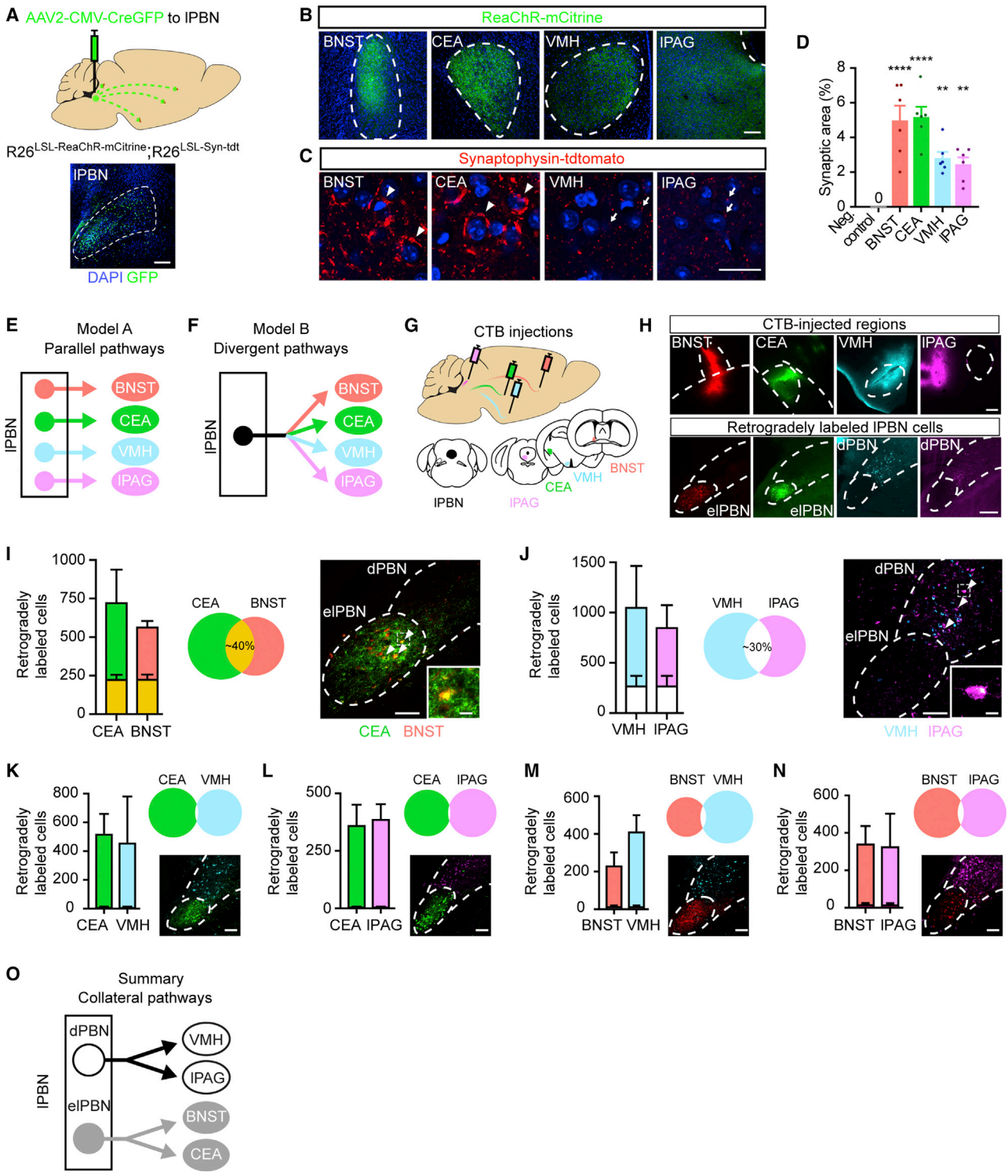

Figure 2. Distinct Subpopulations of lPBN Collateralize to Different Forebrain Regions

(A) Strategy to visualize lPBN neurons, their projections, and their presynaptic terminals. Scale bar, 100 μm.

(B) Projections of lPBN efferents to four different brain regions, as visualized with ReaChR-mCitrine: BSNT, CEA, VMH, and lPAG. Scale bar, 100 μm. Images are representative of results from 6 mice.

(C) Synaptic terminals of lPBN efferents at four indicated targets, as visualized with synaptophysin-tdTomato. Scale bar, 25 μm. Arrowheads and arrows denote perisomatic and diffuse input, respectively.

(legend continued on next page)

(CNO) significantly attenuated acute (capsaicin-induced) and prolonged (complete Freund's adjuvant [CFA]-induced) mechanical hypersensitivity (Figures 1E and 1F). Thus, activity in the lPBN is required for full manifestation of behavioral responses to ongoing pain.

The lPBN is thought to be involved in the aversive aspects of pain: enabling escape behaviors to avoid further tissue injury, mediating descending modulation to facilitate escape in the face of injury, and promoting avoidance learning to avoid future injury. Consistent with these ideas, hM4D-mediated inhibition of the lPBN significantly reduced the degree to which mice jumped away from a heat source (Figure 1G). Although control mice show conditioned pain modulation to a noxious stimulus, this top-down inhibition of the tail flick response was no longer observed upon inhibition of the lPBN (Figures 1H and 1I). Finally, control mice showed conditioned place aversion to a noxious stimulus. However, chemogenetic inhibition of the lPBN during the conditioning phase attenuated learning of this negative association (Figures 1J and 1K). Taken together, these data suggest that activity in the lPBN is important to help an organism escape from a noxious stimulus and to learn avoidance.

Given the necessity of the lPBN for these behavioral responses to noxious stimulation, we next explored the efferent targets from this nucleus. Toward this end, an AAV encoding a Cre-GFP fusion protein was stereotaxically delivered into the lPBN of mice harboring two Cre-dependent alleles: ReaChR-mCitrine for the purpose of visualizing axonal projections and synaptophysin-tdTomato for the purpose of visualizing presynaptic terminals (Figure 2A). We observed lPBN efferent projections to numerous regions of the brain (Figure S2), consistent with previous studies (Bernard et al., 1994, 1996; Gauriau and Bernard, 2002; Saper and Loewy, 1980). Although some inhibitory projections from the lPBN (as assessed using the *Gad2*^{Cre} allele) were observed in most of these target areas, the vast majority of the output appeared to be excitatory (Figure S2). The lPBN outputs targeted four brain regions in particular, as visualized by robust projections from mCitrine-labeled axons and dense puncta from tdTomato-labeled synaptic terminals: the BNST, CEA, VMH, and lPAG (Figures 2B, 2C, S2C, and S2D). Quantification revealed that all four of these regions received significant synaptic input from the lPBN (Figure 2D), although the apparent perisomatic input to the BNST and CEA (arrows) was qualitatively different from the diffuse input observed within the VMH and lPAG (arrowheads in Figures 2D and S2E). Together, these data indicate that the BNST, CEA, VMH, and lPAG are four principle efferent targets of the lPBN.

Next we considered whether there might be parallel pathways originating from distinct cell types within the lPBN (Figure 2E). This model would be consistent with previous work suggesting that distinct subdivisions of the lBPN have distinct projection patterns (Fulwiler and Saper, 1984; Saper and Loewy, 1980). Alternatively, we also considered the possibility of a single major output from the lPBN with multiple targets (Figure 2F). To distinguish between these possibilities, we characterized the projections from the lPBN using the cholera toxin B subunit (CTB) as a retrograde tracing tool (Figure 2G). Intriguingly, we found that stereotaxic injection of the CTB into distinct lPBN targets labeled neuronal cell bodies in different sub-regions of the lPBN: retrograde tracing from the BNST or CEA resulted in labeled neurons within the external lateral division (elPBN), whereas retrograde tracing from the VMH or lPAG labeled neurons within the dorsal division (dPBN) (Figure 2H). These findings suggest the existence of at least two populations of efferent neurons with distinct targets.

Next we performed dual retrograde labeling experiments from different downstream targets in the same animals. Following dual targeting of the CEA and BNST, we found that ~40% of labeled neurons in the lPBN exhibited double labeling with CTB-conjugated fluorophores (Figure 2I). Analogously, dual injection into the VMH and lPAG resulted in ~30% of CTB-containing neurons in the lPBN with double labeling (Figure 2J). In contrast, there was almost no double labeling of lPBN neurons upon dual injection into any of the other four pairwise combinations (Figures 2K–2N). Together, these data define two major efferent pathways from the lPBN: one originating from the dPBN that collateralizes to the VMH and lPAG and a second arising from the elPBN that collateralizes to the BNST and CEA (Figure 2O).

In light of these findings, we next determined whether distinct outputs from the lPBN mediate different components of the nocifensive response. To address this question, we targeted the lPBN with AAVs encoding ChR2 or eYFP and implanted optical fibers above distinct efferent targets, enabling pathway-selective stimulation (Figures 3A and S3A–S3L). Several lines of evidence suggest that the nociceptive threshold is determined, at least in part, by descending modulation from brain structures such as the PAG, which are activated by ascending nociceptive circuitry (Basbaum and Fields, 1978). Moreover, our experiments

(D) Quantification of synaptic input. The relative number of synapses from lPBN was estimated by quantifying the area of synaptophysin-tdTomato expression within the indicated target. An arbitrary brain region with no synaptophysin-tdTomato expression was used as a negative control. Data are mean ± SEM, and dots represent data points from individual animals (n = 6 mice). Asterisks indicate a region significantly different from the negative control region (one-way RM ANOVA followed by Holm-Sidak post hoc test, **$p < 0.01$, ****$p < 0.001$).
(E and F) Models illustrating lPBN efferents as parallel (E) or divergent pathways (F).
(G) Strategy to retrogradely label lPBN efferents with fluorophore-conjugated CTB.
(H) CTB injections into efferent targets (top) and retrogradely labeled cells (bottom) in the elPBN (BSNT and CEA) and dPBN (VMH and lPAG). Scale bars, 100 μm.
(I) Dual injection of CTB into the CEA (green) and BNST (red) resulted in a colocalized signal in approximately 40% of retrogradely labeled cells (yellow) across the entire lPBN. Data are mean ± SEM (n = 4 mice). Arrows highlight co-labeled cells. Scale bar, 50 μm. Magnification is shown in the inset. Scale bar, 10 μm.
(J) Dual injections of CTB into the VMH (blue) and lPAG (purple) resulted in a colocalized signal in 30% of retrogradely labeled cells (white) across the entire lPBN. Data are mean ± SEM (n = 4 mice). Arrows highlight co-labeled cells. Scale bar, 50 μm. Magnification is shown in the inset. Scale bar, 10 μm.
(K–N) Very few dual-labeled neurons were observed following dual CTB injections into the CEA and VMH (K), CEA and lPAG (L), BNST and VMH (M), or BNST and lPAG (N). Data are mean ± SEM (n = 3–4 mice). Scale bars, 50 μm.
(O) Summary illustrating two collateral pathways emerging from the lPBN.

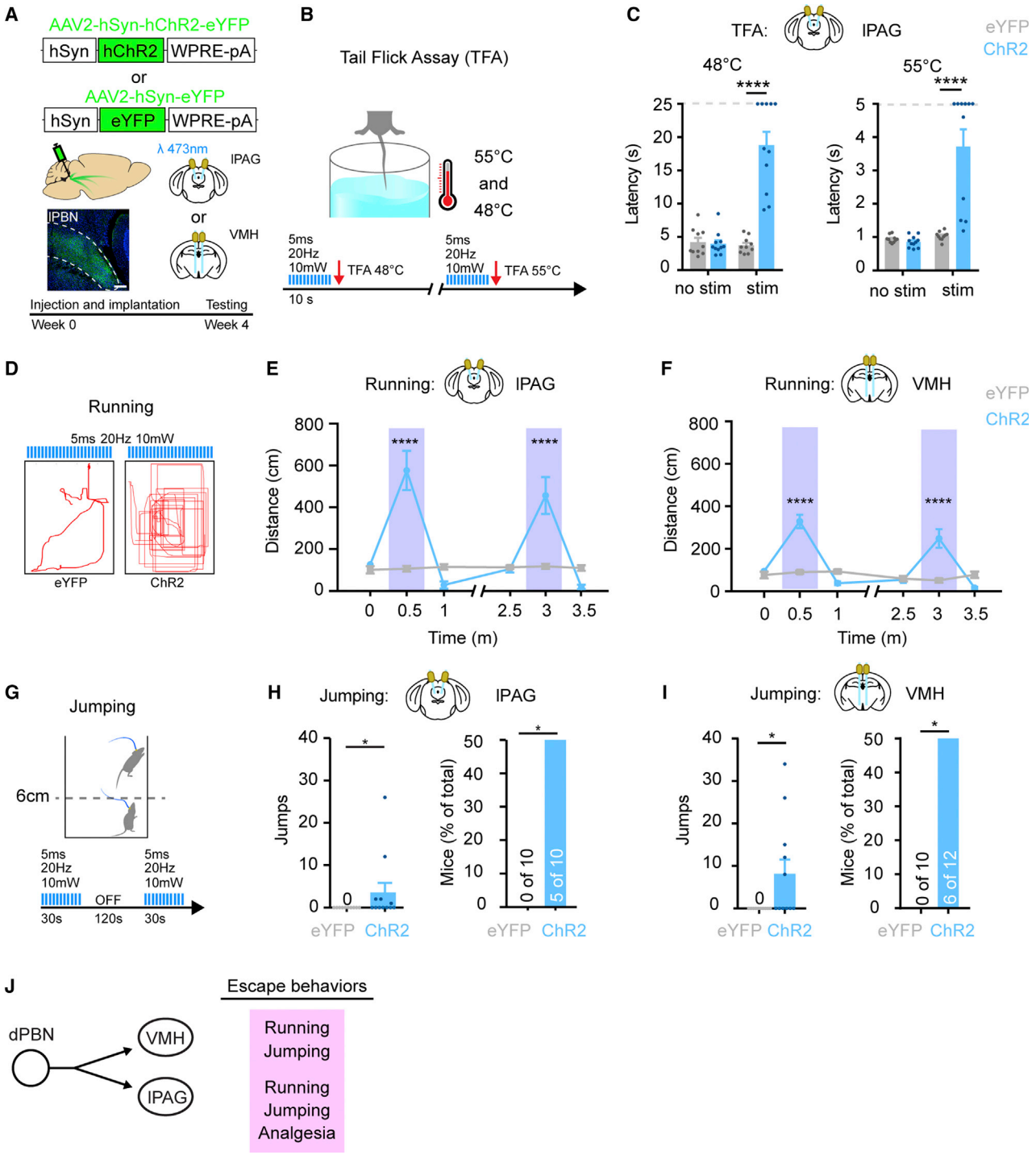

Figure 3. Efferent dPBN Projections to the VMH and lPAG Elicit Escape-like Behaviors

(A) Strategy to selectively activate distinct lPBN projections. AAVs encoding ChR2 or eYFP were injected into the lPBN, and optical implants were placed above one of four efferent targets: lPAG, VMH, CEA, or BNST.

(B) Protocol for the tail flick assay (TFA). Mice were photostimulated for 10 s immediately prior to the TFA at 48°C or 55°C.

(C) Photostimulation of dPBN terminals in the lPAG significantly increased latency to tail flick. Data are mean ± SEM, and dots represent data points from individual animals (n = 9–11 mice per group). Two-way RM ANOVA followed by Holm-Sidak post hoc test, ****$p < 0.0001$. Dotted lines indicate cutoff latencies that were imposed to prevent tissue damage.

(D) Protocol and example traces for the running assay.

(legend continued on next page)

suggested that the lPBN is required for conditioned pain modulation, which is mediated by descending inhibition (Figure 1I). To explore whether any of the efferent projections from the lPBN are sufficient to activate descending inhibition, we assessed whether optogenetic stimulation affected the latency to withdraw in the tail flick assay, which measures a spinal reflex to noxious heat (Figure 3B). Following optogenetic activation of dPBN projections to the lPAG, ChR2-expressing mice showed a significant increase in tail flick latency (Figure 3C), with over half of these mice reaching a cutoff imposed to prevent tissue damage. In contrast, photostimulation of projections to other efferent targets had either no significant effect (VMH or CEA) or only a small effect (BNST) (Figures S4M–S4O). Thus, activation of the efferent pathway from the lPBN to the lPAG is sufficient to elicit robust analgesia through descending inhibition.

Over the course of these studies, we noted that activation of some efferent pathways elicited motor behaviors. To examine this phenomenon in more detail, we quantified the lateral (Figure 3D, running) and vertical (Figure 3G, jumping) movements that were observed upon optogenetic stimulation. Activation of the efferent projection from the dPBN to the lPAG resulted in explosive running behavior that was time locked to the light stimulus (Figure 3E; Video S1). Likewise, stimulation of the projection to the VMH elicited dramatic increases in locomotion that was also time locked to photostimulation (Figure 3F). In contrast, optogenetic activation of efferent projections to the CEA caused no significant lateral movement (Figure S4P), and that to the BNST showed significant lateral movement to the first stimulation only (Figure S4Q). Thus, efferent projections from the dPBN were distinctive in their ability to elicit switch-like locomotor behavior in response to repeated stimulation.

Analogous results were found in the jumping assay, where significant effects were observed upon activation of efferents originating from the dPBN but not the elPBN. Upon activation of projections to the lPAG or the VMH, a significant proportion of mice (50%) jumped as many as 35 times over 1 min of stimulation (Figures 3H and 3I; Video S2). In contrast, jumping behavior upon activation of the efferent pathways to the BNST or the CEA was not significantly different than that observed in eYFP controls (Figures S4R and S4S). Taken together, these findings suggest that the efferent pathways emanating from the dPBN are sufficient to elicit a group of behaviors—running, jumping, and analgesia—that would enable escape in the context of injury or other threats (Figure 3J).

Another important component of the response to noxious input is aversion, which provides a salient cue to enable avoidance learning. We therefore addressed the degree to which activating efferent pathways from the lPBN elicited avoidance using a real-time place aversion assay (Figure 4A). Regardless of which lPBN efferent pathway was targeted, ChR2-expressing mice spent significantly less time on the side of the chamber in which they received photostimulation (Figures 4B–4F). Although this behavior was suggestive of aversion, we also considered the possibility that, at least in some instances (i.e., the VMH and PAG), this apparent avoidance could simply be a consequence of optogenetically induced locomotion. Thus, we assessed whether activation of efferent pathways from the lPBN was sufficient to enable associative conditioning. To accomplish this, we selectively paired optogenetic stimulation with one of two sides of a chamber in a conditioned place aversion (CPA) assay (Figure 4G). When activation of efferent projections to either the CEA or the BNST was the conditioning stimulus, ChR2-expressing mice spent significantly less time on the stimulation-paired side of the chamber (Figures 4H and 4I). In contrast, repeated photostimulation of efferent projections to the VMH or the lPAG failed to induce CPA (Figures S4A and S4B). These findings suggest that, although activation of any of the major outputs from the lPBN gives rise, directly or indirectly, to real-time place aversion, only those projecting to the CEA or BNST are sufficient for stable aversive learning. To further explore how quickly the mice learned to avoid the stimulation-paired side of the chamber in which they received optogenetic stimulation, we re-analyzed the real-time place aversion data, quantifying the number of entries into the light-paired chamber. Photostimulation of the efferent projection to the CEA significantly reduced the number of entries into the stimulation-paired chamber (Figure 4J), whereas activation of other efferent projections had no significant effect on entries (Figures S4C–S4E). Together, these data suggest that avoidance memory can be elicited by efferent pathways from the elPBN (Figure 4K), consistent with previous studies (Campos et al., 2018; Chen et al., 2018; Han et al., 2015; Sato et al., 2015).

Having examined the outputs from the lPBN that could mediate the behavioral responses to noxious stimuli, we next characterized the nociceptive inputs to this nucleus. Toward this end, we used the *Tacr1*^{CreER} allele (Huang et al., 2016) to visualize neurokinin 1 receptor-expressing spinoparabrachial neurons, which are known to transmit noxious signals from the spinal cord to the brain (Cameron et al., 2015; Todd, 2010). To visualize the innervation of the lPBN by these neurons, an AAV encoding a Cre-dependent fluorescent reporter was injected into the L4–L6 region of the spinal cord of *Tacr1*^{CreER} mice

(E) Photostimulation of dPBN terminals in the lPAG significantly increased locomotion. Data are mean ± SEM (n = 9–11 mice per group). Two-way ANOVA followed by Holm-Sidak post hoc test, ****$p < 0.0001$.
(F) Photostimulation of dPBN terminals in the VMH significantly increased locomotion. Data are mean ± SEM (n = 10–12 mice per group). Two-way ANOVA followed by Holm-Sidak post hoc test, ****$p < 0.0001$.
(G) Experimental protocol for the jumping assay. A minimum of 6-cm vertical movement of the body was considered a jump.
(H) Photostimulation of dPBN terminals in the lPAG elicited significant jumping. Data are mean ± SEM, and dots represent data points from individual animals (n = 9–11 mice per group). Left: an asterisk indicates a significant number of jumps (Mann-Whitney test, *$p < 0.05$). Right: an asterisk indicate a significant proportion of mice (Fisher's exact test, *$p < 0.05$).
(I) Photostimulation of dPBN terminals in the VMH elicited significant jumping. Data are mean ± SEM, and dots represent data points from individual animals (n = 9–11 mice per group). Left: an asterisk indicates a significant number of jumps (Mann-Whitney test, *$p < 0.05$). Right: an asterisk indicates a significant proportion of mice (Fisher's exact test, *$p < 0.05$).
(J) Summary of behavioral responses observed upon stimulation of dPBN efferents to the VMH and lPAG.

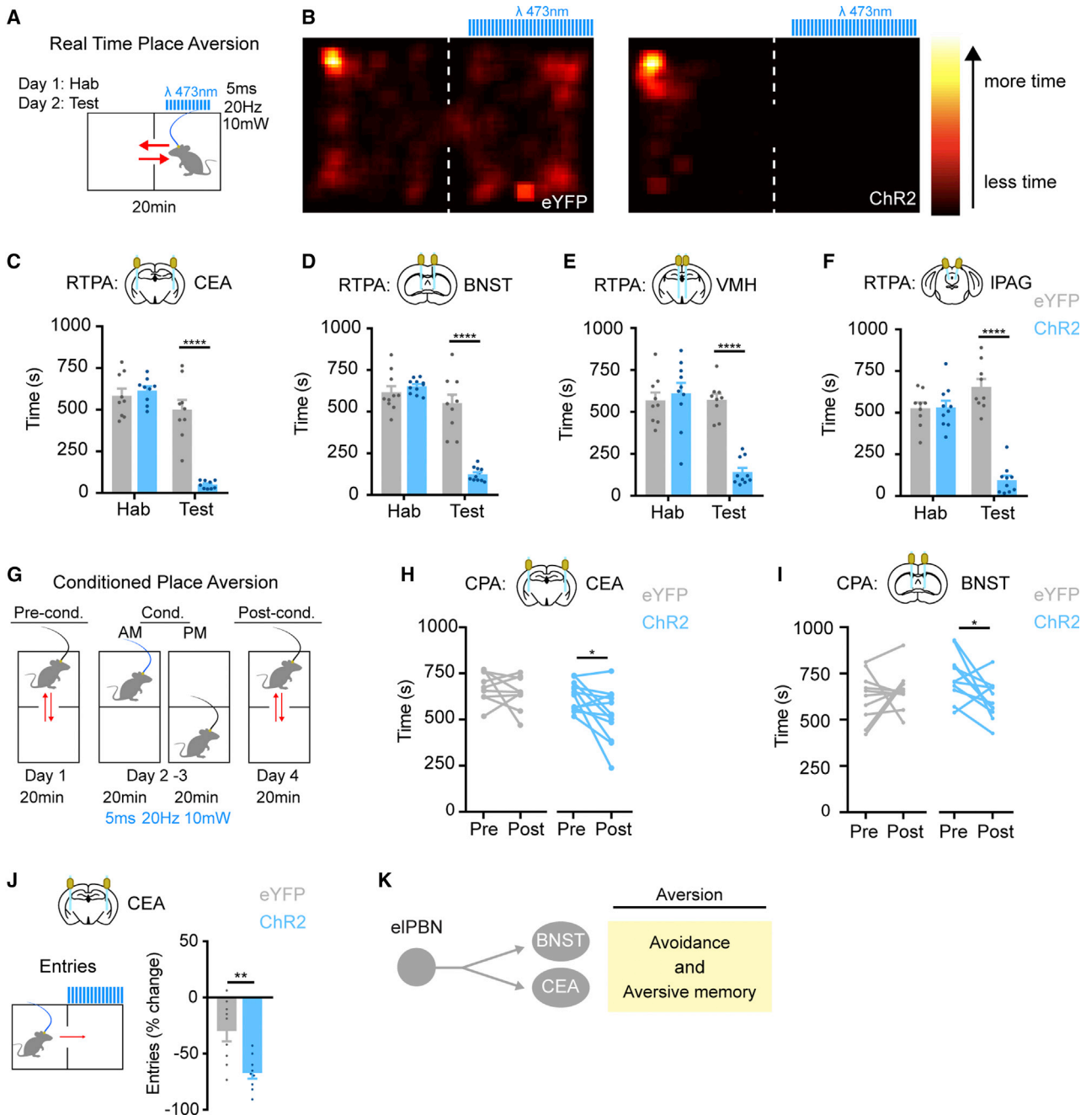

Figure 4. Efferent elPBN Projections to the BNST and CEA Drive Aversion

(A) Protocol for real-time place aversion (RTPA) assay. Mice were habituated (habituation [Hab]) for 20 min 1 day prior to testing.

(B) Heatmaps of time spent in RTPA chambers upon stimulation of lPBN terminals.

(C–F) Time spent in the photostimulation chamber during the Hab phase and testing phase upon stimulation of lPBN efferent terminals in the CEA (C), BNST (D), VMH (E), or lPAG (F). Data are mean ± SEM, and dots represent data points from individual animals (n = 9–11 mice per group for each experiment). Asterisks indicate that ChR2 mice are significantly different from eYFP controls (two-way RM ANOVA followed by Holm-Sidak post hoc test, ****$p < 0.0001$).

(G) Protocol for CPA.

(H and I). Photostimulation of elPBN efferent terminals in the CEA (H) or BNST (I) induced CPA. Data are from individual animals (n = 11–12 mice per group). Paired Student's t test, *$p < 0.05$.

(J) Entries into the photostimulation chamber upon photostimulation of elPBN efferent terminals in CEA terminals. Asterisks indicate that a change in entry number between the test phase and Hab phase is significantly different between eYFP and ChR2 mice (unpaired Student's t test, **$p < 0.01$).

(K) Summary of behavioral responses observed upon stimulation of elPBN outputs to the BNST and CEA.

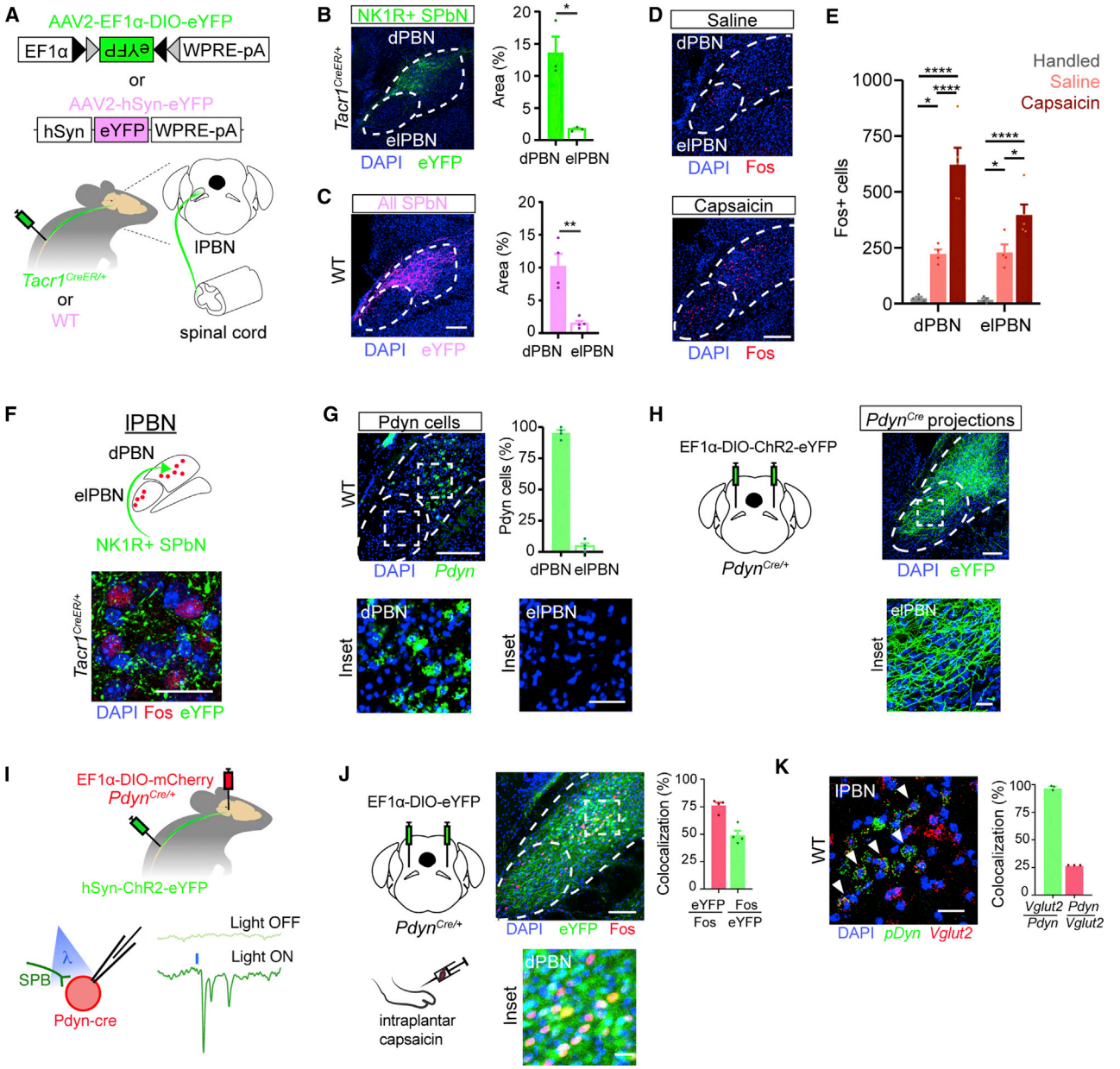

Figure 5. Spinoparabrachial Input Is Concentrated in the dPBN, but Noxious Stimulation Drives Fos Expression in the dPBN and elPBN, Indicating Possible Involvement of Pdyn Neurons.

(A) Strategy to visualize Tacr1 (green) or all (pseudocolored pink) spinal inputs into the lPBN.

(B and C) Representative images and quantification of innervation density of efferent terminals in the lPBN from *Tacr1*^{CreER} (B) or all spinoparabrachial neurons (C). Data are mean ± SEM, and dots represent data points from individual animals (n = 3 mice). Asterisks indicate that the area of spinoparabrachial neuron (SPbN) projections to the dPBN (as percent of region) is significantly greater than that to the elPBN (paired Student's t test, *p < 0.05, **p < 0.01). Scale bar, 100 μm.

(D and E) Representative images (D) and quantification (E) of Fos induction in the dPBN and elPBN in response to intraplantar saline (10 μL) or capsaicin (10 μL, 0.03%). Data are mean ± SEM, and dots represent data points from individual animals (n = 4–5 mice per group). Two-way RM ANOVA followed by Tukey's post hoc test; *p < 0.05, ****p < 0.001. Scale bar, 100 μm.

(F) *Tacr1*$^{CreER/+}$ spinoparabrachial terminals are found in close apposition to Fos+ cells in the dPBN following intraplantar capsaicin. Image is representative of data from 4 mice. Scale bar, 25 μm.

(G) Representative image and quantification of *Pdyn*^{Cre}-expressing neurons in the dPBN and elPBN as visualized by FISH (n = 4 mice). Scale bars, 100 μm; inset, 25 μm.

(H) *Pdyn*^{Cre} neurons in the dPBN project to the elPBN. Images are representative of data from at least 4 mice. Scale bars, 100 μm; inset, 25 μm.

(I) Strategy to optogenetically activate spinal projections onto *Pdyn*^{Cre} dPBN neurons.

(legend continued on next page)

(Figure 5A). We found that *Tacr1*^{CreER} neurons showed dense innervation of the lPBN that was regionally constrained, with the vast majority of these terminals targeting the dPBN and very few targeting the elPBN (Figure 5B), consistent with previous studies (Harrison et al., 2004). To ensure that this observation was not specific to *Tacr1*^{CreER} neurons, we repeated this experiment using a constitutive AAV to label all spinoparabrachial neurons. Again, we saw the same distribution of input from the spinal cord, which was predominant in the dPBN but not the elPBN (Figure 5C).

The paucity of direct nociceptive input to the elPBN was somewhat curious to us in light of previous studies that showed direct innervation of elPBN neurons by spinoparabrachial neurons (Cechetto et al., 1985; Feil and Herbert, 1995; Ma and Peschanski, 1988). Indeed, we found that the dPBN and elPBN subregions showed significant Fos induction in response to noxious stimulation induced via capsaicin treatment of the hindpaw (Figures 5D and 5E), consistent with previous results (Bernard et al., 1994; Hermanson and Blomqvist, 1996). However, the presynaptic terminals of *Tacr1*^{CreER} spinoparabrachial neurons were only observed in close apposition to Fos+ neurons within the dPBN (Figure 5F).

The apparent discrepancy between the localized nature of the nociceptive input in the dPBN and the widespread nature of the Fos induction by intraplantar capsaicin raised the question of how noxious information reaches the elPBN. With the goal of identifying a neuronal population that might convey nociceptive information between lPBN subregions, we investigated cell types that are known to be expressed in the dPBN using a combination of Cre alleles (*Sst*^{Cre}, *Calb2*^{Cre}, *Crh*^{Cre}, *Tacr1*^{CreER}, *Nts*^{Cre}, and *Pdyn*^{Cre}) and stereotaxic injection of Cre-dependent AAV reporters. Although all of these genetic tools uncovered populations of neurons with subregion-specific expression in the lPBN, only the dynorphin population showed a localization and anatomy that positioned them to convey noxious information from the dPBN to the elPBN (Figure S5A). In particular, using dual FISH, we found that *Pdyn* neurons were located almost exclusively in the dPBN (Figure 5G), consistent with previous studies (Geerling et al., 2016). Next we validated the *Pdyn*^{Cre} allele, confirming that Cre-dependent AAV viruses injected into the lPBN of these mice selectively targeted *Pdyn*-expressing neurons (Figure S5B). Finally, we found that dynorphin-expressing neurons in the dPBN send dense projections to the elPBN (Figure 5H) but fewer to other major efferent targets (Figure S5C). Thus, dynorphin-expressing neurons have cell bodies in the dPBN and send prominent projections to the elPBN.

Next we investigated whether spinoparabrachial neurons provide input onto the *Pdyn*^{Cre} subset of dPBN neurons. In slice experiments, we found that optogenetic activation of spinoparabrachial terminals gave rise to excitatory postsynaptic currents (EPSCs) in eYFP-labeled *Pdyn*^{Cre} neurons with a latency that was suggestive of direct input (Figures 5I and S5D–S5F). Moreover, intraplantar injection of capsaicin gave rise to strong Fos induction in *Pdyn*^{Cre} neurons. Specifically, 75% of Fos-expressing cells belonged to the *Pdyn*^{Cre} population, and Fos was induced in 50% of these cells (Figure 5J). Together, these data provide physiological and functional evidence that *Pdyn*^{Cre} neurons in the dPBN receive noxious input via spinoparabrachial neurons.

To characterize these *Pdyn*^{Cre} neurons in more detail, we examined whether they are excitatory or inhibitory neurons through dual FISH. We found that nearly all *Pdyn* transcripts colocalized with *Vglut2*, with *Pdyn* cells representing approximately one-quarter of the excitatory population within the dPBN (Figure 5K). In contrast, there was very little to no overlap of *Pdyn* and the inhibitory marker *Vgat* (Figure S5G). Thus, from a neurochemical standpoint, dynorphin neurons in the dPBN are positioned to relay nociceptive information to the elPBN.

We next investigated whether dynorphin neurons could provide a cellular substrate for transmission of nociceptive information to elPBN efferents. We used viral and retrograde tracing approaches to visualize presynaptic puncta from *Pdyn*^{Cre} neurons in close proximity to elPBN neurons that project to the CEA and BNST (Figure S5H). These experiments suggested that approximately two-thirds of CTB-labeled cells from the BNST or the CEA showed close apposition of retrogradely labeled cells to synaptophysin-eYFP and the post-synaptic density marker Homer1 (Figures S5I and S5J). Intriguingly, we did not find evidence of direct excitatory connections between these cells and CEA-projecting elPBN efferents in optogenetic experiments, raising the possibility that the regulation of elPBN output by *Pdyn*^{Cre} neurons may involve more complex circuit mechanisms such as presynaptic modulation onto elPBN neurons (Figures S5K–S5O).

Next we investigated how the ChR2-mediated manipulation of *Pdyn*^{Cre} neurons in the dPBN affected the behavioral responses that are mediated by elPBN efferents (Figure 6A). We found that photostimulation of *Pdyn*^{Cre} neurons in lPBN mice was sufficient for aversive behaviors but not escape behaviors. In particular, optogenetic stimulation resulted in real-time place aversion coupled with a significant reduction in number of entries into the stimulation chamber (Figures 6B and 6C). In contrast, activation of *Pdyn*^{Cre} neurons had no effect on escape behaviors, including running, jumping, or tail flick latency (Figures S6A–S6C). To examine whether *Pdyn*^{Cre} neurons in the dPBN are required for pain-induced aversive learning, we used a caspase-based strategy to selectively ablate this population (Figures 6D–6F and S6D–S6I). Next we used a CPA assay in which a noxious stimulus (2% intraplantar formalin, 10 μL) was selectively paired with one of the two chambers for 20 min (Figure 6G). eYFP-expressing control mice spent significantly less time on the formalin-paired side of the chamber, whereas those in which *Pdyn*^{Cre} neurons in the dPBN were ablated failed to show CPA (Figure 6H). In contrast, ablation of *Pdyn*^{Cre} neurons in the dPBN had no effect

(J) *Pdyn*^{Cre} dPBN neurons express Fos following intraplantar capsaicin (10 μL, 0.03%). Data are mean ± SEM, and dots represent data points from individual animals (n = 4 mice). Scale bars, 25 μm; inset, 5 μm.

(K) *Pdyn*^{Cre} dPBN neurons are primarily excitatory. Shown are a representative image and quantification of colocalization between *Pdyn* and *Vglut2* mRNA in the dPBN, as observed by dual FISH. Data are mean ± SEM, and dots represent data points from individual animals (n = 3 mice). Arrowheads denote neurons with colocalized signals. Scale bar, 25 μm.

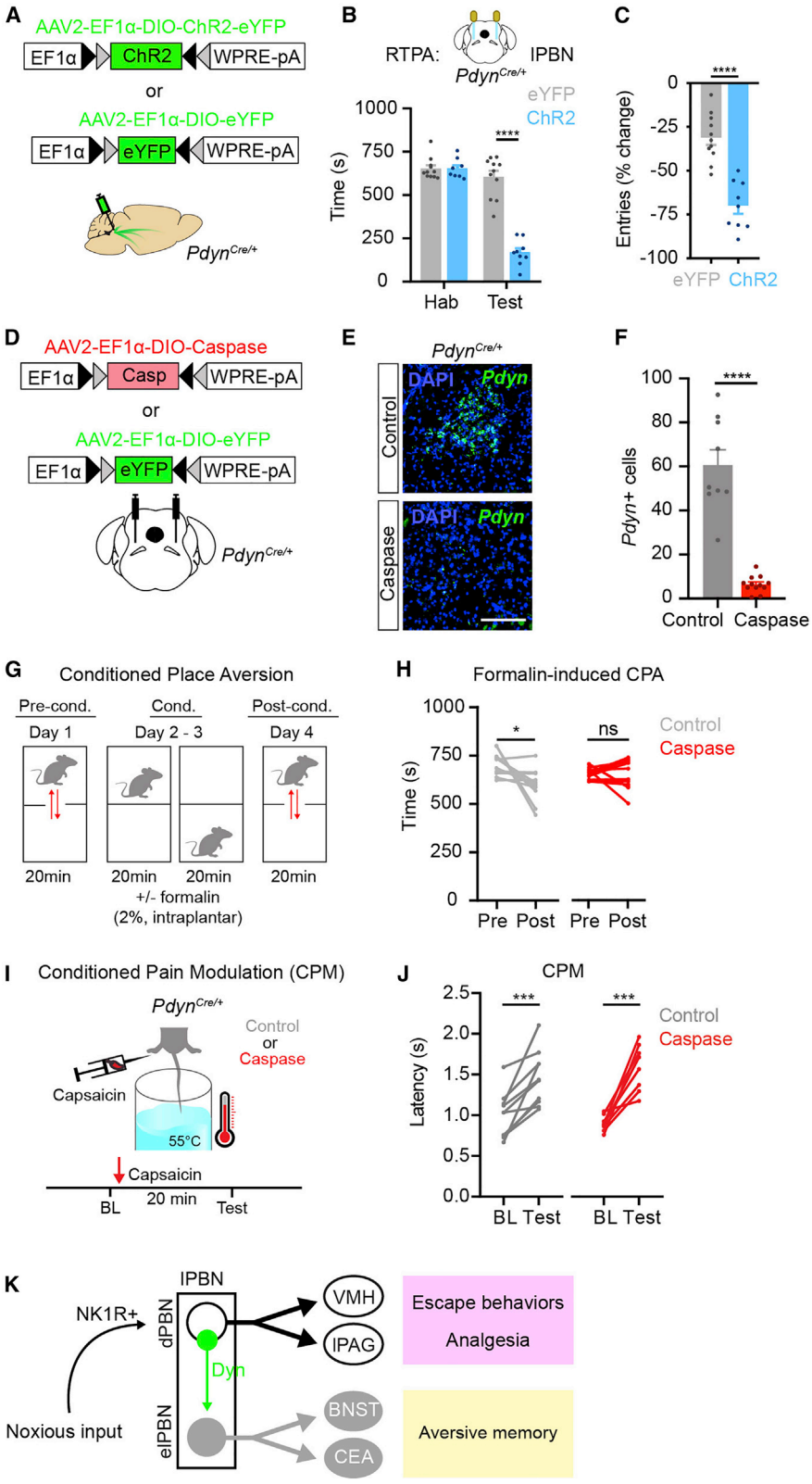

(legend on next page)

on an assay for conditioned pain modulation, (Figures 6I and 6J), arguing that this ablation did not affect the efferent pathway from the dPBN to the PAG. Taken together, these findings suggest that *Pdyn*^{Cre} neurons serve as a crucial link for recruitment of elPBN pathways to the CEA and BNST (Figure 6K).

DISCUSSION

We have identified two anatomically and functionally distinct populations of lPBN neurons that underlie different aspects of the nocifensive response. Neurons in the dPBN receive direct input from spinal projection neurons and mediate behaviors that would enable escape, whereas neurons in the elPBN mediate aversive learning. In addition, we provide evidence that *Pdyn* neurons, which span these divisions of the PBN, are required for aversive learning.

It is intriguing that distinct lPBN efferents would be predicted to have opposite effects on behavioral responses to noxious stimuli; those emanating from the dorsal division would be expected to decrease pain, whereas those from the external lateral domain would be expected to exacerbate pain. The efferent pathway from the dPBN might predominate in the context of an emergency to help avoid injury, whereas the efferent pathway from the elPBN might predominate when imminent danger has passed to facilitate aversive learning. The neural substrate for coordination of different efferent responses in this way is poorly understood. Our work suggests that *Pdyn*^{Cre} neurons may be involved in this coordinated regulation between efferent projections emanating from the dorsal and external lateral domains, respectively. Our data reveal that *Pdyn*^{Cre} neurons have cell bodies in the dPBN but send extensive projections to the elPBN, and, consistent with this anatomy, we find that these cells are activated by noxious input and drive aversion but not escape behaviors. However, this is unlikely to be the only function of *Pdyn*^{Cre} neurons in the lPBN because these neurons have been shown to play important roles in temperature homeostasis (Geerling et al., 2016; Nakamura and Morrison, 2008, 2010). These findings indicate that *Pdyn*^{Cre} neurons in the lPBN are not a single homogeneous population. In future studies, it will be important to characterize this heterogeneity in more detail to identify *bona fide* cell types and characterize how each responds to diverse stimuli.

Coordination of behavioral and physiological adaptations under dangerous or potentially dangerous scenarios is critical for an animal's survival. In the context of nociceptive stimuli, humans more than any other species have a detailed cortical representation that informs conscious perception of pain. However, this cortico-centric view of pain may overlook the fundamental idea that avoiding tissue damage is a primal need in which subcortical pathways play a central role. Our studies highlight a potentially important role of dynorphin in the lPBN in this regulation. Because chronic pain has such a profound effect on mental health and well-being, further studies investigating changes in this circuitry in the context of chronic pain and the possible role of dynorphin signaling therein are warranted.

STAR★METHODS

Detailed methods are provided in the online version of this paper and include the following:

- KEY RESOURCES TABLE
- RESOURCE AVAILABILITY
  - Lead Contact
  - Materials Availability
  - Data and Code Availability
- EXPERIMENTAL MODEL AND SUBJECT DETAILS
- METHOD DETAILS
  - Viruses
  - Stereotaxic injections and implantation of optical fiber
  - RNAscope *in situ* hybridization
  - Immunohistochemistry
  - CTB backlabeling
  - Image acquisition and quantification
  - Tamoxifen induction
  - Fos induction (intraplantar capsaicin)
  - Opto Fos
  - Behavior
  - Real time place aversion assay (RTPA)
  - Tail immersion test
  - Thermal escape response test
  - Optogenetic escape response test

Figure 6. Dynorphin-Expressing Neurons May Convey Nociceptive Input from the dPBN to the elPBN

(A) Strategy to express optogenically activated *Pdyn*^{Cre} lPBN neurons.

(B) Photostimulation of ChR2-expressing *Pdyn*^{Cre} cells in the dPBN elicited RTPA. Data are mean ± SEM, and dots represent data points from individual animals (n = 9–11 mice per group). Two-way RM ANOVA followed by Holm-Sidak post hoc test, ****$p < 0.0001$.

(C) Photostimulation of ChR2-expressing *Pdyn*^{Cre} cells in the dPBN significantly diminished entries into the stimulation chamber. Data are mean ± SEM, and dots represent data points from individual animals (n = 9–11 mice per group). Unpaired Student's t test, ****$p < 0.0001$.

(D) Strategy to ablate *Pdyn*^{Cre} neurons in the lPBN.

(E) Example image of *Pdyn*^{Cre} lPBN neurons following injection of a control and a caspase virus. Scale bar, 100 μm.

(F) Caspase mice exhibited significantly fewer *Pdyn*^{Cre} neurons. Data are mean ± SEM and dots represent data points from individual animals (n = 9–12 mice per group). Unpaired Student's t test, ****$p < 0.0001$.

(G) Strategy to test for CPA. Mice were conditioned to 2% intraplantar formalin and one side of a two-chambered box differentiated by visual cues.

(H) Formalin-induced CPA was no longer observed upon loss of *Pdyn*^{Cre} neurons (n = 11–12 mice per group). *$p < 0.05$; ns, $p > 0.05$; paired Student's t test.

(I) Strategy to test for CPM. Mice were treated with a control or a caspase virus and tested in a TFA following intraplantar capsaicin injection.

(J) CPM was observed regardless of loss of *Pdyn*^{Cre} neurons (n = 8–10 mice per group) ****$p < 0.0001$, ***$p < 0.001$ (paired Student's t test).

(K) Model. Noxious input is conveyed primarily to the dPBN. Efferents from the dPBN collateralize to the VMH and lPAG and mediate behavioral responses that enable escape. Dynorphin neurons in the dPBN convey noxious information to the elPBN. Efferents from the elPBN collateralize onto the CEA and BNST and mediate aversion and avoidance memory.

- Conditioned place aversion
- Conditioned Pain Modulation
- Mechanical allodynia
- Intraspinal injections
- Electrophysiology

● QUANTIFICATION AND STATISTICAL ANALYSIS

SUPPLEMENTAL INFORMATION

Supplemental Information can be found online at https://doi.org/10.1016/j.neuron.2020.03.014.

ACKNOWLEDGMENTS

We thank Hannah E. Piston for generating equipment for the tail flick assay and Michael S. Gold for helpful comments. The research reported in this publication was supported by the Virginia Kaufman Endowment Fund, NIH/NIAMS grant AR063772, and NIH/NINDS grant NS096705 (to S.E.R.); NRSA F30 grant F30NS096860 and NIGM/NIH T32GM008208 (to M.C.C.); CRCNS NIDCD R01DC015139 (to A.-M.M.O.); and Consejo Nacional de Ciencia y Tecnología (CONACYT) Convocatoria 291258 (to M.C.-B.).

AUTHOR CONTRIBUTIONS

Conceptualization, M.C.C. and S.E.R.; Methodology, M.C.C., E.K.N., A.E.P., and S.E.R.; Investigation, M.C.C. and S.E.R.; Writing, M.C.C. and S.E.R.; Electrophysiology, M.C.-B. and A.-M.M.O.; Funding Acquisition, M.C.C. and S.E.R.

DECLARATION OF INTERESTS

The authors declare no competing interests.

Received: April 2, 2019
Revised: November 20, 2019
Accepted: March 16, 2020
Published: April 13, 2020

REFERENCES

Al-Khater, K.M., and Todd, A.J. (2009). Collateral projections of neurons in laminae I, III, and IV of rat spinal cord to thalamus, periaqueductal gray matter, and lateral parabrachial area. J. Comp. Neurol. *515*, 629–646.

Alhadeff, A.L., Su, Z., Hernandez, E., Klima, M.L., Phillips, S.Z., Holland, R.A., Guo, C., Hantman, A.W., De Jonghe, B.C., and Betley, J.N. (2018). A Neural Circuit for the Suppression of Pain by a Competing Need State. Cell *173*, 140–152.e15.

Barik, A., Thompson, J.H., Seltzer, M., Ghitani, N., and Chesler, A.T. (2018). A Brainstem-Spinal Circuit Controlling Nocifensive Behavior. Neuron *100*, 1491–1503.e3.

Basbaum, A.I., and Fields, H.L. (1978). Endogenous pain control mechanisms: review and hypothesis. Ann. Neurol. *4*, 451–462.

Ben-Shaul, Y. (2017). OptiMouse: a comprehensive open source program for reliable detection and analysis of mouse body and nose positions. BMC Biol. *15*, 41.

Bernard, J.F., Huang, G.F., and Besson, J.M. (1994). The parabrachial area: electrophysiological evidence for an involvement in visceral nociceptive processes. J. Neurophysiol. *71*, 1646–1660.

Bernard, J.F., Bester, H., and Besson, J.M. (1996). Involvement of the spino-parabrachio -amygdaloid and -hypothalamic pathways in the autonomic and affective emotional aspects of pain. Prog. Brain Res. *107*, 243–255.

Bester, H., Besson, J.M., and Bernard, J.F. (1997). Organization of efferent projections from the parabrachial area to the hypothalamus: a Phaseolus vulgaris-leucoagglutinin study in the rat. J. Comp. Neurol. *383*, 245–281.

Cameron, D., Polgár, E., Gutierrez-Mecinas, M., Gomez-Lima, M., Watanabe, M., and Todd, A.J. (2015). The organisation of spinoparabrachial neurons in the mouse. Pain *156*, 2061–2071.

Campos, C.A., Bowen, A.J., Roman, C.W., and Palmiter, R.D. (2018). Encoding of danger by parabrachial CGRP neurons. Nature *555*, 617–622.

Cechetto, D.F., Standaert, D.G., and Saper, C.B. (1985). Spinal and trigeminal dorsal horn projections to the parabrachial nucleus in the rat. J. Comp. Neurol. *240*, 153–160.

Chamberlin, N.L., and Saper, C.B. (1994). Topographic organization of respiratory responses to glutamate microstimulation of the parabrachial nucleus in the rat. J. Neurosci. *14*, 6500–6510.

Chaplan, S.R., Bach, F.W., Pogrel, J.W., Chung, J.M., and Yaksh, T.L. (1994). Quantitative assessment of tactile allodynia in the rat paw. J. Neurosci. Methods *53*, 55–63.

Chen, J.Y., Campos, C.A., Jarvie, B.C., and Palmiter, R.D. (2018). Parabrachial CGRP Neurons Establish and Sustain Aversive Taste Memories. Neuron *100*, 891–899.e5.

Chiang, M.C., Bowen, A., Schier, L.A., Tupone, D., Uddin, O., and Heinricher, M.M. (2019). Parabrachial Complex: A Hub for Pain and Aversion. J. Neurosci. *39*, 8225–8230.

Espejo, E.F., and Mir, D. (1993). Structure of the rat's behaviour in the hot plate test. Behav. Brain Res. *56*, 171–176.

Fan, R.J., Shyu, B.C., and Hsiao, S. (1995). Analysis of nocifensive behavior induced in rats by CO2 laser pulse stimulation. Physiol. Behav. *57*, 1131–1137.

Feil, K., and Herbert, H. (1995). Topographic organization of spinal and trigeminal somatosensory pathways to the rat parabrachial and Kölliker-Fuse nuclei. J. Comp. Neurol. *353*, 506–528.

Fulwiler, C.E., and Saper, C.B. (1984). Subnuclear organization of the efferent connections of the parabrachial nucleus in the rat. Brain Res. *319*, 229–259.

Gauriau, C., and Bernard, J.F. (2002). Pain pathways and parabrachial circuits in the rat. Exp. Physiol. *87*, 251–258.

Geerling, J.C., Kim, M., Mahoney, C.E., Abbott, S.B., Agostinelli, L.J., Garfield, A.S., Krashes, M.J., Lowell, B.B., and Scammell, T.E. (2016). Genetic identity of thermosensory relay neurons in the lateral parabrachial nucleus. Am. J. Physiol. Regul. Integr. Comp. Physiol. *310*, R41–R54.

Han, S., Soleiman, M.T., Soden, M.E., Zweifel, L.S., and Palmiter, R.D. (2015). Elucidating an Affective Pain Circuit that Creates a Threat Memory. Cell *162*, 363–374.

Harrison, T.A., Hoover, D.B., and King, M.S. (2004). Distinct regional distributions of NK1 and NK3 neurokinin receptor immunoreactivity in rat brainstem gustatory centers. Brain Res. Bull. *63*, 7–17.

Hermanson, O., and Blomqvist, A. (1996). Subnuclear localization of FOS-like immunoreactivity in the rat parabrachial nucleus after nociceptive stimulation. J. Comp. Neurol. *368*, 45–56.

Hermanson, O., and Blomqvist, A. (1997). Subnuclear localization of FOS-like immunoreactivity in the parabrachial nucleus after orofacial nociceptive stimulation of the awake rat. J. Comp. Neurol. *387*, 114–123.

Hooks, B.M., Lin, J.Y., Guo, C., and Svoboda, K. (2015). Dual-channel circuit mapping reveals sensorimotor convergence in the primary motor cortex. J. Neurosci. *35*, 4418–4426.

Huang, H., Kuzirian, M.S., Cai, X., Snyder, L.M., Cohen, J., Kaplan, D.H., and Ross, S.E. (2016). Generation of a NK1R-CreER knockin mouse strain to study cells involved in Neurokinin 1 Receptor signaling. Genesis *54*, 593–601.

Huang, T., Lin, S.H., Malewicz, N.M., Zhang, Y., Zhang, Y., Goulding, M., LaMotte, R.H., and Ma, Q. (2019). Identifying the pathways required for coping behaviours associated with sustained pain. Nature *565*, 86–90.

Jansen, N.A., and Giesler, G.J., Jr. (2015). Response characteristics of pruriceptive and nociceptive trigeminoparabrachial tract neurons in the rat. J. Neurophysiol. *113*, 58–70.

Kaur, S., Pedersen, N.P., Yokota, S., Hur, E.E., Fuller, P.M., Lazarus, M., Chamberlin, N.L., and Saper, C.B. (2013). Glutamatergic signaling from the parabrachial nucleus plays a critical role in hypercapnic arousal. J. Neurosci. *33*, 7627–7640.

Kaur, S., Wang, J.L., Ferrari, L., Thankachan, S., Kroeger, D., Venner, A., Lazarus, M., Wellman, A., Arrigoni, E., Fuller, P.M., et al. (2017). A Genetically Defined Circuit for Arousal from Sleep during Hypercapnia. Neuron *96*, 1153–1167.e5.

Krashes, M.J., Shah, B.P., Madara, J.C., Olson, D.P., Strochlic, D.E., Garfield, A.S., Vong, L., Pei, H., Watabe-Uchida, M., Uchida, N., et al. (2014). An excitatory paraventricular nucleus to AgRP neuron circuit that drives hunger. Nature *507*, 238–242.

Kunwar, P.S., Zelikowsky, M., Remedios, R., Cai, H., Yilmaz, M., Meister, M., and Anderson, D.J. (2015). Ventromedial hypothalamic neurons control a defensive emotion state. eLife *4*.

Le Bars, D., Gozariu, M., and Cadden, S.W. (2001). Animal models of nociception. Pharmacol. Rev. *53*, 597–652.

Liu, A., Papale, A.E., Hengenius, J., Pate, K., Ermentrout, B., and Urban, N.N. (2019). Mouse navigation strategies for odor source localization. bioRxiv. https://doi.org/10.1101/2019.11.11.558643.

Ma, W., and Peschanski, M. (1988). Spinal and trigeminal projections to the parabrachial nucleus in the rat: electron-microscopic evidence of a spino-ponto-amygdalian somatosensory pathway. Somatosens. Res. *5*, 247–257.

Menendez, L., Bester, H., Besson, J.M., and Bernard, J.F. (1996). Parabrachial area: electrophysiological evidence for an involvement in cold nociception. J. Neurophysiol. *75*, 2099–2116.

Nakamura, K., and Morrison, S.F. (2008). A thermosensory pathway that controls body temperature. Nat. Neurosci. *11*, 62–71.

Nakamura, K., and Morrison, S.F. (2010). A thermosensory pathway mediating heat-defense responses. Proc. Natl. Acad. Sci. USA *107*, 8848–8853.

Palmiter, R.D. (2018). The Parabrachial Nucleus: CGRP Neurons Function as a General Alarm. Trends Neurosci. *41*, 280–293.

Rodriguez, E., Sakurai, K., Xu, J., Chen, Y., Toda, K., Zhao, S., Han, B.X., Ryu, D., Yin, H., Liedtke, W., and Wang, F. (2017). A craniofacial-specific monosynaptic circuit enables heightened affective pain. Nat. Neurosci. *20*, 1734–1743.

Saper, C.B. (2016). The House Alarm. Cell Metab. *23*, 754–755.

Saper, C.B., and Loewy, A.D. (1980). Efferent connections of the parabrachial nucleus in the rat. Brain Res. *197*, 291–317.

Sato, M., Ito, M., Nagase, M., Sugimura, Y.K., Takahashi, Y., Watabe, A.M., and Kato, F. (2015). The lateral parabrachial nucleus is actively involved in the acquisition of fear memory in mice. Mol. Brain *8*, 22.

Taniguchi, H., He, M., Wu, P., Kim, S., Paik, R., Sugino, K., Kvitsiani, D., Fu, Y., Lu, J., Lin, Y., et al. (2011). A resource of Cre driver lines for genetic targeting of GABAergic neurons in cerebral cortex. Neuron *71*, 995–1013.

Todd, A.J. (2010). Neuronal circuitry for pain processing in the dorsal horn. Nat. Rev. Neurosci. *11*, 823–836.

Todd, A.J., McGill, M.M., and Shehab, S.A. (2000). Neurokinin 1 receptor expression by neurons in laminae I, III and IV of the rat spinal dorsal horn that project to the brainstem. Eur. J. Neurosci. *12*, 689–700.

Wang, L., Chen, I.Z., and Lin, D. (2015). Collateral pathways from the ventromedial hypothalamus mediate defensive behaviors. Neuron *85*, 1344–1358.

Zeng H. (2011). Direct Data Submission 2011/04/15 MGI Direct Data Submission MGI: J:170755.

STAR★METHODS

KEY RESOURCES TABLE

REAGENT or RESOURCE	SOURCE	IDENTIFIER
Antibodies		
Rabbit anti-homer 1	Frontier Institute	Cat: AB_2571774; RRID: AB_2571774
Chicken anti-GFP	Aves Laboratory	Cat: GFP-1020; RRID: AB_10000240
Rabbit anti-c-fos	Santa Cruz Biotech	Cat: Sc-52; RRID: AB_216783
Rabbit anti-NK1R	Sigma Aldrich	Cat: SAB4502913; RRID: AB_10746598
Donkey anti-chicken (IgG) Alexa Fluor 488 secondary antibody	Jackson ImmunoResearch	Cat: 703-035-155; RRID: AB_2340375
Donkey anti-rabbit (IgG) Alexa Fluor 555 secondary antibody	ThermoFisher	Cat: A-31572; RRID: AB_162543
Bacterial and Virus Strains		
AAV2-hSyn-eYFP	UNC	Addgene: Cat: 50465
AAV2-hSyn.hChR2(H134R).eYFP	UNC	Addgene: Cat: 26973
AAV2-EF1a-DIO-eYFP	UNC	Addgene: Cat: 27056
AAV2-EF1a-DIO-hChR2(H134R)-eYFP	UNC	Addgene: Cat: 20298
AAV2-EF1a-flex-taCasp3-TEVp	UNC	Addgene: Cat: 45580
AAV5-CaMKIIa-mCherry	UNC	NA
AAV5-CaMKIIa-hM4D(Gi)-mCherry	Roth Lab DREADDs	Addgene: Cat: 50477
AAV8.2-hEF1a-DIO-synaptophysin-eYFP	MGH GTC	Cat: AAV-RN2
AAV8.2-hEF1a-synaptophysin-mCherry	MGH GTC	Cat: AAV-RN8
AAV9-CAGGS-FLEX-ChR2-tdtomato.WRPE.SV40	Penn Vector Core	Addgene: Cat: 18917
Chemicals, Peptides, and Recombinant Proteins		
Cholera toxin subunit B (Recombinant), Alexa Fluor 555	ThermoFisher	Cat: C34778
Cholera toxin subunit B (Recombinant), Alexa Fluor 647	ThermoFisher	Cat: C22843
Clozapine N-oxide (CNO)	ThermoFisher	Cat: 6329
Complete Freund's adjuvant (CFA)	Sigma Aldrich	Cat: F5881
PFA	Sigma Aldrich	Cat: P6148
Capsaicin	Sigma Aldrich	Cat: M2028
Formalin	Sigma Aldrich	Cat: HT501128
Tamoxifen	Sigma Aldrich	Cat: T5648-5G
Corn oil	Sigma Aldrich	Cat: C8267
Critical Commercial Assays		
RNAscope		N/A
Fluorescent multiplex assay	ACD	Cat: 320850
Pdyn probe	ACD	Cat: 318771
Calca probe	ACD	Cat: 417961
Tac1 probe	ACD	Cat: 410351
Gad2 probe	ACD	Cat: 415071
Fos probe	ACD	Cat: 316921
Slc32a1 probe	ACD	Cat: 319191
Slc17a6 probe	ACD	Cat: 319171
EYFP probe	ACD	Cat: 312131
DAPI	ACD	Cat: 320858

(*Continued on next page*)

Continued

REAGENT or RESOURCE	SOURCE	IDENTIFIER
3-plex positive control probe	ACD	Cat: 320881
3-plex negative control probe	ACD	Cat: 320871
Experimental Models: Organisms/Strains		
Mouse: C57BL6	Charles River	Cat: 027
Mouse: Pdyn-IRES-Cre B6;129S-Pdyntm1.1(cre)Mjkr/LowlJ	Jackson Laboratory (Krashes et al. 2014)	IMSR Cat: JAX:027958; RRID: IMSR_ JAX:027958
Mouse: Gad2-IRES-Cre Gad2tm2(cre)Zjh/J	Jackson Laboratory (Taniguchi et al., 2011)	IMSR Cat: JAX:010802; RRID: IMSR_ JAX:010802
Mouse: Tacr1CreER	Ross lab (Huang et al., 2016)	N/A
Mouse: Ai34D or Ai34(RCL-Syp/tdT)-D B6;129S-Gt(ROSA)26Sortm34.1(CAG-Syp/tdTomato)Hze/J	Jackson Laboratory (Zeng, 2011)	IMSR Cat: JAX:012570; RRID: IMSR_ JAX:012570
Mouse: Rosa26 CAG-LSL-ReaChR-mCit B6.Cg-Gt(ROSA)26Sortm2.2Ksvo/J	Jackson Laboratory (Hooks et al., 2015)	IMSR Cat: JAX:026294; RRID: IMSR_ JAX:026294
Software and Algorithms		
Prism 7.0	GraphPad	https://www.graphpad.com/scientific-software/prism/
MATLAB	Mathworks	https://www.mathworks.com/
Mouse tracking algorithm	Liu et al., 2019	N/A

RESOURCE AVAILABILITY

Lead Contact

Further information and requests for resources and reagents should be directed to and will be fulfilled by the Lead Contact, Sarah Ross (saross@pitt.edu)

Materials Availability

This study did not generate new unique reagents.

Data and Code Availability

Custom-written MATLAB code and data for in this study are available from the lead contact upon request.

EXPERIMENTAL MODEL AND SUBJECT DETAILS

Mice were given free access to food and water and housed under standard laboratory conditions. The use of animals was approved by the Institutional Animal Care and Use Committee of the University of Pittsburgh. *Pdyn-IRES-Cre* (Krashes et al., 2014), *Gad2-IRES-Cre* (Taniguchi et al., 2011), *Tacr1-CreER* (Huang et al., 2016), Ai34 *(RCL-Syp/tdT)-D*, *Sst-Cre* (Taniguchi et al., 2011), *Calb2-Cre* (Taniguchi et al., 2011), *Crh-Cre* (Taniguchi et al., 2011), *Nts-Cre*, and *Rosa26 CAG-LSL-ReaChR-mCit* (Hooks et al., 2015) were obtained from Jackson Laboratory. Wild-type C57BL/6 mice were obtained from Charles River (Cat # 027). For all experiments 8- to 16-week-old male and female mice were used. In all cases, no differences between male and female mice were observed and so the data were pooled. Age-matched littermates were used for all behavioral experiments that involved mice harboring the knock-in allele Cre-recombinase.

METHOD DETAILS

Viruses

The following viruses were used for experimentation: AAV2-hsyn-eYFP (Addgene: 50465), AAV2-hSyn-hChR2(H134R)-eYFP (Addgene: 26973), AAV2-EF1a-DIO-eYFP (Addgene: 27056), AAV2-EF1a-DIO-hChR2(H134R)-eYFP (Addgene: 20298), AAV9-CAGGS-FLEX-ChR2-tdtomato.WRPE.SV40 (Addgene: 18917), AAV5-CaMKIIa-hM4D(Gi)-mCherry (Addgene: 50477), AAV2-EF1a-flex-taCasp3-TEVp (Addgene: 45580), AAV8.2-hEF1a-DIO-synaptophysin-eYFP (MGH: AAV-RN2),and AAV8.2-hEF1a-synaptophysin-mCherry (MGH: AAV-RN8). Viruses were purchased from University of North Carolina Vector Core, University of Pennsylvania Vector Core, and Massachusetts Gene Technology Core.

Stereotaxic injections and implantation of optical fiber

Animals were anesthetized with 2% isoflurane and placed in a stereotaxic head frame. Ophthalmic ointment was applied to the eyes. The scalp was shaved, local antiseptic applied (betadine), and a midline incision made to expose the cranium. The skull was aligned using cranial fissures. A drill bit (MA Ford, #87) was used to create a burr hole and custom-made metal needle (33 gauge) loaded with virus was subsequently inserted through the hole to the injection site. Virus was infused at a rate of 100nL/min using a Hamilton syringe with a microsyringe pump (World Precision Instruments). Wild-type mice received 0.150 μL of virus. All other Cre-expressing mice received 0.5 μL virus. The injection needle was left in place for an additional 5-10 min and then slowly withdrawn. Injections and optical fiber implantations were performed bilaterally at the following coordinates for each brain region: BNST: AP +0.50 mm, ML ± 1.00 mm, DV −4.30; CEA: AP −1.20 mm, ML ± 2.85 mm, DV −4.50; VMH: AP −1.48 mm ML ± −0.50 mm DV −5.80 mm; lPAG: AP −4.70 mm, ML ± 0.74 mm, DV: −2.75; and lPBN AP −5.11 mm, ML ± 1.25 mm, DV: −3.25. For implantation of optical fibers (Thor Labs: 1.25 mm ceramic ferrule 230 μm diameter), implants were slowly lowered 0.3 - 0.5 mm above the site of injection and secured to the skull with a thin layer of Vetbond (3M) and dental cement. The incision was closed using Vetbond and animals were given a subcutaneous injection of buprenorphine (0.3mg/kg) and allowed to recover over a heat pad. Mice were given 4 weeks to recover prior to experimentation.

RNAscope *in situ* hybridization

Multiplex fluorescent *in situ* hybridization was performed according to the manufacturer's instructions (Advanced Cell Diagnostics #320850). Briefly, 18 μm-thick fresh-frozen sections containing the parabrachial nucleus were fixed in 4% paraformaldehyde, dehydrated, treated with protease for 15 minutes, and hybridized with gene-specific probes to mouse *Pdyn* (#318771), *Calca* (#417961), *Tac1* (#410351), *Fos* (#316921), *Slc32a1* (#319191), and *Slc17a6* (#319171). DAPI (#320858) was used to visualize nuclei. 3-plex positive (#320881) and negative (#320871) control probes were tested. Two to three full-thickness z stacked sections were quantified for a given mouse, and 2 - 4 mice were used per experiment.

Immunohistochemistry

Mice were anesthetized with an intraperitoneal injection of urethane, transcardially perfused, and post-fixed at least four hours in 4% paraformaldehyde. 40 or 65 μm thick transverse brain or spinal cord sections were collected on a vibratome and processed free-floating for immunohistochemistry. Sections were blocked at room temperature for two hours in a 10% donkey serum, 0.1% triton, 0.3M NaCl in phosphate buffered saline. Primary antibodies were incubated for 14 hours overnight at 4°C (except for rabbit anti-Homer1, detailed below): rabbit anti-c-Fos (1:5K), chicken anti-GFP (1:1K), rabbit anti-NK1R (1:1K), and rabbit anti-Homer1 (1:1K, incubated for 3 days). Sections were subsequently washed three times for 20 minutes in wash buffer (1% donkey serum, 0.1% triton, 0.3M NaCl) and incubated in secondary antibodies (Life Technologies, 1:500) at room temperature for two hours. Sections were then incubated in Hoechst (ThermoFisher, 1:10K) for 1 minute and washed 7 times for 15 minutes in wash buffer, mounted and coverslipped.

CTB backlabeling

Fluorescently conjugated cholera toxin subunit B-Alexa Fluor conjugates −555 and −647 (CTB, ThermoFisher C34778, C22843) were stereotactically injected (0.2 μl, 1mg/ml) into the brain regions of interest and subsequently analyzed 10 days following injection. Mice were perfused and brains were processed as described above for immunohistochemistry. CTB-labeled cells were quantified using 65 μm z stacked images at 2 μm steps of the entire lPBN (n = 3 – 5 mice per backlabeled region). For retrograde labeling of cells and quantification of pre- and post-synaptic markers, 3 – 4 40 μm sections were quantified for a given animal, and 4 mice were used per experiment.

Image acquisition and quantification

Full-tissue thickness sections were imaged using either an Olympus BX53 fluorescent microscope with UPlanSApo 4x, 10x, or 20x objectives or a Nikon A1R confocal microscope with 20X or 60X objectives. All images were quantified and analyzed using ImageJ. For all images, background pixel intensity was subtracted as calculated from control mice. To quantify the area of synapses observed, confocal images using single optical planes were converted into a binary scale and area of signal taken as a ratio of the total area (one section per region of interest, n = 6 mice). To quantify CTB-labeled cells in tracing experiments, confocal images were manually quantified using full-tissue thickness z stacked images at 2 μm steps of the entire lPBN (3 – 4 mice per group). To quantify images in RNAscope *in situ* hybridization experiments, confocal images of tissue samples (1 – 2 sections per mouse over 2 – 4 mice) were imaged and only cells whose nuclei were clearly visible by DAPI staining and exhibited fluorescent signal were counted. To quantify Fos-labeled cells, 65 μm sections of the entire lPBN were imaged using the fluorescent microscope and images manually counted.

Tamoxifen induction

Tacr1-CreER mice between 8-9 weeks of age were treated with 20 mg/ml concentration of tamoxifen dissolved in filtered corn oil (0.20 μm sterile syringe filter, Corning 431224) over 5 consecutive days at 75 mg/kg.

Fos induction (intraplantar capsaicin)

Fos induction was performed as previously described in Rodriguez et al. (2017). Mice were lightly anesthetized with isoflurane and received one of the following treatments: handled (no injection), 10 μL unilateral intraplantar saline, or 10 μL unilateral intraplantar capsaicin (0.03% capsaicin w/v in 2.5% Tween 80 and 2.5% ethanol in PBS). Mice were then placed back into their cages and subsequently perfused 90 minutes later and neural tissue collected according to protocol for immunohistochemistry.

Opto Fos

To induce Fos in optically implanted mice for OptoFos experiments, mice were photostimulated at 10 mW, 20 Hz, and 5 ms pulse duration for 20 minutes at a 3 s on, 2 s off stimulation pattern and subsequently perfused 90 minutes after the initial onset of photostimulation as noted for immunohistochemistry. 65 μm thick transverse sections of brain were collected on a vibratome and processed free-floating for immunohistochemistry as detailed in STAR Methods. To quantify Fos-labeled cells, 3 optical planes separated by 10 μm from the center of each section was merged into a single layer and counted for each region of interest (lPBN, BNST, CEA, VMH, and lPAG).

Behavior

All assays were performed and scored by an experimenter blind to virus (eYFP or ChR2). Post hoc analysis confirming specificity of viral injections and proper fiber implantation were also performed blinded to animal identity, and mice in which viral injections and/or fiber implantation were considered off target excluded from analysis. All testing was performed in the University of Pittsburgh Rodent Behavior Analysis Core. Optogenetic stimulation parameters were determined empirically as follows: 10mW, 20Hz, 5ms duration pulses.

Real time place aversion assay (RTPA)

Mice were stereotaxically injected with either channelrhodopsin or control eYFP virus and optical fibers implanted at the downstream terminals of interest. Four weeks following injection mice were habituated to a custom-made 2-chamber (40 cm x 28 cm x 20 cm chamber) for RTPA testing. Mice were habituated on day 1 for 20 minutes and subsequently tested the next day for 20 minutes. Light stimulation was delivered whenever the mouse entered one of two sides of the chamber and turned off when the animal exited that chamber. The side of stimulation was counterbalanced. The behavior was recorded and post hoc analysis performed to determine body position using the open source software Optimouse (Ben-Shaul, 2017). Position data were discarded according to established criteria (Liu et al., 2019).

Tail immersion test

Mice were habituated to mice restraints 15 minutes for 5 days before testing. Tails were immersed 3 cm into a water bath at 48°C or 55°C, and the latency to tail flick was measured three times per temperature with a one-minute interval between trials. For optogenetic testing, mice were photostimulated for 10 s prior to tail immersion testing.

Thermal escape response test

Following a 30-minute pretreatment with CNO (5 mg/kg), mice were placed on a 55°C hotplate. The latency to first jump and total number of jumps over 60 s period were measured. Values were averaged across two trials for each mouse.

Optogenetic escape response test

Mice were placed in an open field chamber and allowed to habituate for five minutes before two 30 s optogenetic stimulation bouts and one-minute resting periods between bouts. The behavior was recorded and post hoc analysis performed to determine body position using the open source software Optimouse as described in RTPA.

Conditioned place aversion

Mice were placed in a two-chamber plexiglass box for 20 minutes and allowed to freely roam between one of two sides differentiated by visual cues (spots versus stripes). For two conditioning days, mice were restricted to one of two sides and received either no stimulation or photostimulation (3 s on, 2 s off at 20 Hz, 5 ms pulse duration, 10 mW) for 20-minute periods in the morning and afternoon. On the test day, mice were placed back into the box and allowed to freely explore either chamber. The behavior was recorded and post hoc analysis performed to determine body position using the open source software Optimouse as described in RTPA. For formalin-induced CPA, mice were conditioned to 2% 10 μL solution of formalin injected into either one hindpaw on the first day of conditioning and the contralateral hindpaw on the second day of conditioning. Control mice received no hindpaw injections. In experiments involving hM4D, mice were pretreated with CNO (5 mg/kg) 30 min prior to conditioning with formalin.

Conditioned Pain Modulation

For conditioned pain modulation, mice were injected with 10 μL 0.1% capsaicin solution into the right hindpaw and subsequently tested 20 minutes post-injection at 55°C for tail flick latency as described during the tail immersion test. In experiments involving hM4D, mice were pretreated with CNO (5 mg/kg) 30 min prior to the experiment.

Mechanical allodynia

Mice were allowed to habituate for at least two hours prior to testing. Mice received a 10ul intraplantar injection of 0.03% capsaicin dissolved in 2.5% Tween, 2.5% ethanol in PBS and tested for mechanical hypersensitivity via the up-down method (Chaplan et al., 1994). After a 5- to 10-minute resting period, mice were optogenetically stimulated and tested for mechanical hypersensitivity. Mice were again allowed to rest for 5-10 minutes before von Frey testing for post-stimulation effects on mechanical hypersensitivity. For chemogenetic testing of mechanical hypersensitivity, mice were given an i.p. injection of CNO (5 mg/kg) after intraplantar delivery of 0.03% capsaicin and subsequently tested for mechanical hypersensitivity 20 minutes post injection. To model persistent inflammatory pain, mice were injected with 20 μL of a 1:1 saline solution of Complete Freund's adjuvant (CFA). One week later, mice were tested for mechanical hypersensitivity as described above.

Intraspinal injections

Mice were anesthetized with 100 mg/kg ketamine and 10 mg/kg xylazine. An incision was made at the spinal cord level corresponding to L4-6 dermatome. The intrathecal space was exposed, and two injections of approximately 1 μL of virus was infused 300 μm below the surface of the spinal cord at 100 nL/min via glass pipette through the intrathecal space corresponding to L4-L6 of the spinal cord. The glass pipette was left in place for an additional 5 minutes before withdrawal. The incision was closed with 5-0 vicryl suture. Buprenorphine was delivered post-surgery at 0.3mg/kg subcutaneously, and mice were allowed to recover over a heat pad.

Electrophysiology

Slice Preparation

For some experiments, *Pdyn-Cre* mice (4 - 6 weeks) were stereotaxically injected with EF1a-DIO-mCherry in the PBN to visualize Pdyn neurons and hSyn-ChR2-eYFP into the dorsal spinal cord for ChR2 expression in spinal output neurons. In other experiments, *Pdyn-Cre* mice (4 - 6 weeks) were stereotaxically injected with EF1a-DIO-ChR2 in the PBN and Ctb in the CeA (or BNST). Four weeks later, brains from these mice were freshly dissected and sectioned coronally (200 μm) using a vibratome (Leica Biosystems) in an ice-cold oxygenated low Ca^{2+}, high Mg2+ cutting solution (95% O2%–5% CO2) 125 mM NaCl, 2.5 mM KCl, 25 mM NaHCO3, 1.25 mM NaH2PO4, 3.0 mM MgCl2, 10 mM Dextrose, 0.5 CaCl2). The slices were maintained into this solution at 35°C for 30 min and transferred to warm (32°C) oxygenated (95% O2%–5% CO2) normal ACSF solution (in mM: 125 NaCl, 2.5 KCl, 25 NaHCO3, 1.25 NaH2PO4, 1.0 MgCl2, 25 Dextrose, 2.5 CaCl2) for 45-60 min prior to recording in the same conditions (32°C with normal ACSF).

Recordings

Whole cell, voltage and current clamp recordings were performed using a MultiClamp 700B amplifier (Molecular Devices, Union City, CA). Data were low pass filtered (4 kHz) and digitized at 10 kHz or 5kHz using an ITC-18 (Instrutech) controlled by custom software (Recording Artist, https://bitbucket.org/rgerkin/recording-artist) written in IgorPro (Wavemetrics). Recording pipettes (4-10 MW) were pulled from borosilicate glass (1.5 mm, outer diameter) on a Flaming/Brown micropipette puller (Sutter Instruments). The series resistance (< 20 MW) was not corrected. The intracellular solution consisted of (in mM) 130 K-gluconate, 5 KCl, 2 MgCl2, 4 ATP-Mg, 0.3 GTP, 10 HEPES, and 10 phosphocreatine, 0.05% biocytin. Neurons were visualized using infrared-differential interference contrast and fluorescence microscopy (Olympus, Dage IR camera, Photometrics camera). Suprathreshold action potentials rates were assessed using a series of depolarizing current steps (50 pA, 1 s duration). Voltage clamp recordings of EPSCs were performed at −70 mV holding potential and current clamp EPSP recordings were acquired at resting membrane potential.

Optogenetic Stimulation: Shutter controlled full field light stimulation of blue light (473 nm) provided by a mercury lamp was delivered through the epifluorescence pathway of the microscope (Olympus) using a water-immersion objective (40x). The duration of the light pulse was 1 ms and intensity ranged from 3-5 mW to reliably synaptic evoke responses on repeated trials (10-25, 30-60 s inter-trial interval). EPSC detection, amplitude and delay were analyzed using custom software written in IgorPro (Wavemetrics). Since light stimulation frequently evoked a small number of synaptic responses per trial, evoked EPSCs or EPSPs were analyzed in the first 50 ms following light or electrical stimulation. In unstimulated conditions, (i.e., Control, No Light) the average baseline amplitude was calculated for the same 50 ms window. Reported synaptic latencies and amplitudes for each cell correspond to the trial average of the first EPSP or EPSC following stimulation. All population data is reported as mean+/− SEM

QUANTIFICATION AND STATISTICAL ANALYSIS

All statistical analyses were performed using GraphPad Prism 7.0. Values are presented as mean ± SEM. Statistical significance was assessed using Fisher's exact test for categorical data, Students t test, or two-way repeated-measures ANOVA followed by Holm-Sidak post hoc test. Significance was indicated by $p \leq 0.05$. The n for each experiment is described in the figure legends. Sample sizes were based on pilot data and are similar to those typically used in the field.